Taylor & Francis
Taylor & Francis Group

Canadian Journal of Remote Sensing
Journal canadien de télédétection

ISSN: (Print) (Online) Journal homepage: https://www.tandfonline.com/loi/ujrs20

Landfast Ice Mapping Using MODIS Clear-Sky Composites: Application for the Banks Island Coastline in Beaufort Sea and Comparison with Canadian Ice Service Data

Alexander P. Trishchenko & Yi Luo

To cite this article: Alexander P. Trishchenko & Yi Luo (2021) Landfast Ice Mapping Using MODIS Clear-Sky Composites: Application for the Banks Island Coastline in Beaufort Sea and Comparison with Canadian Ice Service Data, Canadian Journal of Remote Sensing, 47:1, 143-158, DOI: 10.1080/07038992.2021.1909466

To link to this article: https://doi.org/10.1080/07038992.2021.1909466

Published online: 20 Apr 2021.

CANADIAN JOURNAL OF REMOTE SENSING
2021, VOL. 47, NO. 1, 143–158
https://doi.org/10.1080/07038992.2021.1909466

Taylor & Francis
Taylor & Francis Group

Landfast Ice Mapping Using MODIS Clear-Sky Composites: Application for the Banks Island Coastline in Beaufort Sea and Comparison with Canadian Ice Service Data

Cartographie des glaces côtières à l'aide de composites MODIS ciel clair: application pour la côte de l'île Banks en mer de Beaufort et comparaison avec les données du Service canadien des glaces

Alexander P. Trishchenko[a] and Yi Luo[b]

[a]Canada Centre for Remote Sensing, NRCan, Ottawa, ON K1A 0E4, Canada; [b]Canadian Ice Service, ECCC, Ottawa, ON, Canada

ABSTRACT

Landfast ice (LFI) is a prominent climatological feature in the Canadian Arctic. LFI is generally defined as immobile near-shore ice that remains fast along the coast and forms seaward from the land. It affects the coastline dynamics, is important for the near-shore ecosystems, wildlife, and human socio-economic activities. A method is proposed for mapping the LFI using time series of 10-day clear-sky composites derived at the Canada Center for Remote Sensing (CCRS) from the Moderate Resolution Imaging Spectroradiometer (MODIS) 250-m imagery. The delineation of coastal zone ice utilizes simultaneous analysis of the mean and standard deviation of MODIS monthly reflectance maps. The application of this method is demonstrated for a 20-year period (2000–2019) over the coastal zone of Banks Island in the Beaufort Sea. Detailed analyses have been conducted for three LFI parameters: (1) the total area (spatial extent) occupied by LFI; (2) the distance from the coast to the outer seaward LFI edge, and (3) the water depth at the outer seaward LFI edge. Comparison with the Canadian Ice Service (CIS) data demonstrates good agreement. The average correlation coefficients between CIS and CCRS time series in April-June, when the area reaches a maximum, are equal to 0.87–0.88. The mean differences (CIS-CCRS) are 344 km^2 (5,464 km^2 vs 5,120 km^2) or 6.3% for the spatial extent; 1.3 km (17.6 km vs 16.3 km) or 7.4% for the distance; −2.7 m (−27.4 m vs −24.7 m) or 10% for the water depth. Because the CCRS method uses monthly statistics, it tends to exclude potentially more mobile continuous landfast ice zones than the CIS analysis which is based on data collected on a specific date. The long-term trends of the LFI seasonal cycle in our region of interest since 2000 have shown a tendency for an earlier break-up, later onset, and longer ice-free period; however, these trends are not statistically significant.

RÉSUMÉ

La banquise côtière (BC) est une caractéristique climatologique importante de l'Arctique canadien. La BC est généralement définie comme de la glace immobile près du rivage qui reste solide le long de la côte et se forme vers la mer à partir de la terre. Elle affecte la dynamique du littoral et elle est importante pour les écosystèmes côtiers, la faune et les activités socio-économiques humaines. Une méthode est proposée pour cartographier la BC à l'aide de séries chronologiques de composites sous ciel dégagé sur 10 jours produites au Centre canadien de télédétection (CCT) à partir du spectroradiomètre imageur à résolution modérée (MODIS) de 250 m. La délimitation de la glace de la zone côtière utilise l'analyse simultanée de la moyenne et de l'écart type des cartes de réflectance mensuelles MODIS. L'application de cette méthode est démontrée sur une période de 20 ans (2000-2019) sur la zone côtière de l'île Banks dans la mer de Beaufort. Des analyses détaillées ont été menées pour trois paramètres de la BC: 1) la superficie totale (étendue spatiale) occupée par la BC; 2) la distance entre la côte et le bord extérieur de la BC côté mer, et 3) la profondeur de l'eau au bord extérieur de la BC côté mer. La comparaison avec les données du Service canadien des glaces (SCG) démontre une bonne concordance. Les coefficients de corrélation moyens entre les séries chronologiques du SCG et du CCT en avril-juin, lorsque la superficie

ARTICLE HISTORY
Received 18 December 2020
Accepted 11 March 2021

CONTACT Alexander P. Trishchenko alexander.trichtchenko@canada.ca

atteint un maximum, sont égaux à 0,87-0,88. Les différences moyennes (SCG -CCT) sont de 344 km^2 (5464 km^2 vs 5120 km^2) ou 6,3% pour l'étendue spatiale; 1,3 km (17,6 km vs 16,3 km) ou 7,4% pour la distance; −2,7 m (-27,4 m vs −24,7 m) ou 10% pour la profondeur de l'eau. Étant donné que la méthode du CCT utilise des statistiques mensuelles, elle tend à exclure potentiellement plus de zones de glaces continentales continues mobiles que l'analyse du SCG qui est basée sur des données recueillies à une date précise. Les tendances à long terme du cycle saisonnier de la BC dans notre région d'intérêt depuis 2000 ont montré une tendance à une débâcle plus précoce, à un début plus tardif et à une période libre de glace plus longue; cependant, ces tendances ne sont pas statistiquement significatives.

Introduction

The coastline of Banks Island facing the Beaufort Sea is an important Arctic ecosystem (Environment Canada 2015). Landfast ice (LFI) is a prominent climatological feature of this region essential for the local population, wildlife, ecosystem functions, and the state of coastline. According to the Canadian Ice Service (CIS 2009), landfast ice is defined as "*Ice which forms and remains fast along the coast. …. It may be formed 'in-situ' from water or by freezing of floating ice of any age to shore and can extend a few metres or several hundred kilometres from the coast.*" The general climate conditions and some recent impacts of changing climate on Banks Island are described by French (2016) and Fraser et al. (2018). Banks Island is the fourth largest island in the Canadian Arctic with a mixture of polar desert and tundra environments. Climate warming caused widespread ice-wedge degradation that affected more than 3.5% of its total upland area in recent years. As the Arctic continues to warm at a rate twice as high as the global average value (Overland et al. 2019), this warming also has a significant impact on the landfast ice. The climate change impact on landfast ice is one of the greatest factors affecting the Arctic coastal communities (Cooley et al. 2020). Quantitative information about the distribution of coastal zone ice is required to better understand the impacts associated with climatic changes in this Arctic region.

The location of the study area is shown in Figure 1. Panel (a) displays the entire Beaufort Sea region as the melting season (April–September) snow/ice probability map (Trishchenko, Leblanc, et al. 2016; Trishchenko 2020) with an overlaid boundary of the Beaufort Sea and a rectangular box corresponding to the selected coastline zone of Banks Island. The probability map shows the ratio of the number of snow or ice detections to the total number of available observations in the 10-day clear-sky composite time series generated for the April-September season each year. An enlarged picture of the selected study region is shown in Figure 1b as the clear-sky composite image derived from the Moderate Resolution Imaging Spectroradiometer (MODIS) on TERRA spacecraft for the entire month of June 2008. Figure 1b displays the false-color image that uses the following RGB color scheme: MODIS band 1 (visible, VIS: 620–670 nm) reflectance (BLUE), band 2 (near-infrared, NIR: 841–876 nm) reflectance (GREEN), and band 6 (shortwave infrared, SWIR: 1,628–1,652 nm) reflectance (RED). The MODIS imagery has been processed with CCRS-developed technology and downscaled to 250-m spatial resolution as described in the next section. Cyan, blue and turquoise colors in Figure 1b correspond to sea ice and snow. Yellow and brown colors depict the barren arctic landscapes, and black corresponds to open water.

The satellite data displayed in Figure 1 clearly show the systematic presence of sea ice attached to the Banks Island coast. The coastal ice regime along the west coast of Banks Island and the Beaufort Sea region is generally driven by the seasonal cycle of meteorological conditions, the bathymetry of the ocean floor in the shallow water zone, and by a large-scale ocean circulation system persistent over the region known as the Beaufort Gyre (Proshutinsky et al. 2002). The bathymetry of the region and neighboring areas is shown in Figure 2. Bathymetry data have been obtained from the general bathymetric chart of the oceans (GEBCO Compilation Group 2020). The central zone of the Beaufort Sea is very deep, while shallow coastal waters can extend tens of kilometers. The detailed bathymetry map for the west coast of Banks Island is displayed in Figure 3. One can see the extended zone of very shallow waters and sharp gradients of the depth at the southern and especially at the northern boundary of the region in the M'Clure Strait.

Routine operational sea-ice mapping, including the landfast ice, is conducted by the mandated national agencies, such as, the Canadian Ice Service in Canadian Waters (https://www.canada.ca/en/environment-climate-change/services/ice-forecasts-observations.html) and the U.S. National Ice Center (https://www.natice.noaa.gov) that generates global ice charts. The CIS daily and weekly

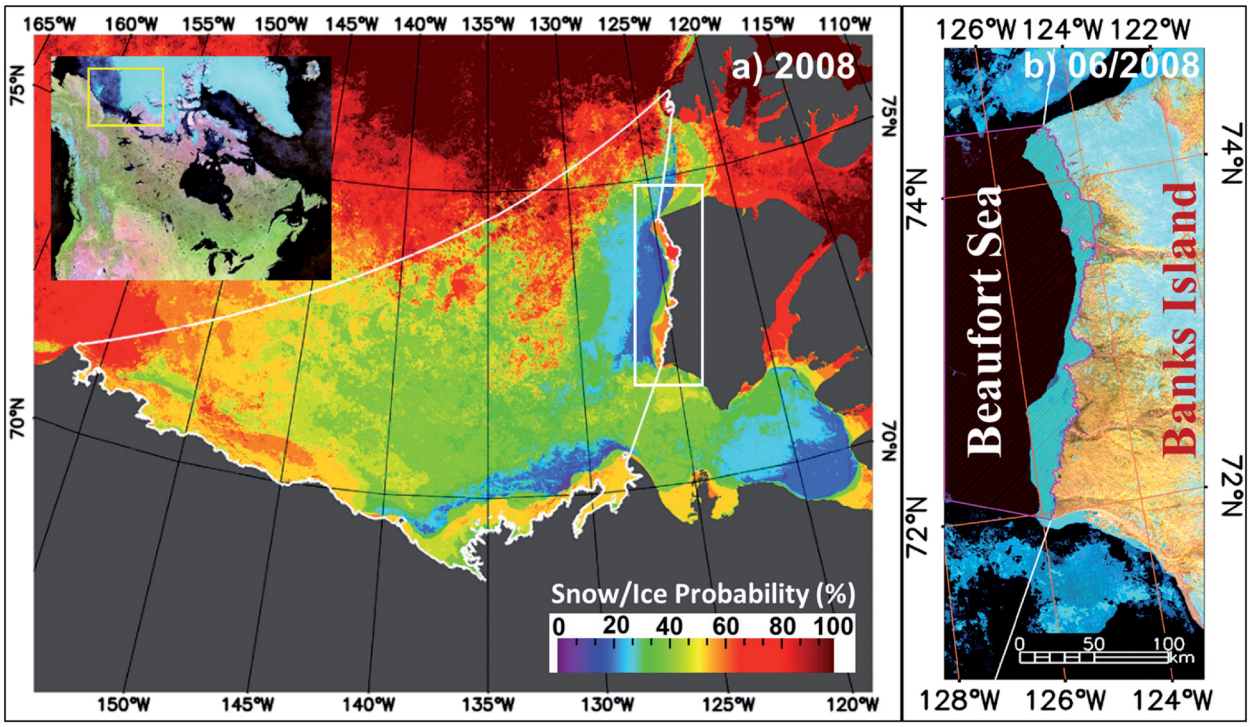

Figure 1. The location of the study region. (a) Example of the 2008 melting season (April–September) snow/ice probability map (Trishchenko, Leblanc, et al. 2016; Trishchenko 2020) for the Beaufort Sea region; (b) Study region: West coast of Banks Island facing the Beaufort Sea from the MODIS monthly clear-sky composite product for June 2008 displayed as a false-color image with RGB using bands B6, B2 and B1. The landfast ice is visible along the Banks Island coastline in the Beaufort Sea. The white contour indicates the boundary of the Beaufort Sea. The white rectangle on panel (a) indicates the extent of the study region which is enlarged on panel (b). The coastal region marked by magenta lines on panel (b) depicts a zone utilized for the analysis of landfast ice. The digital shapefile for the Beaufort Sea has been obtained from the open database published by the Flanders Marine Institute (2019). The snow/ice probability map produced by the Canada Center for Remote Sensing (CCRS) is available from the Canadian Federal Geospatial Platform (FGP) open-access public archive https://open.canada.ca/data/en/dataset/808b84a1-6356-4103-a8e9-db46d5c20fcf.

products represent the best estimates of ice properties at the moment of ice chart production obtained from the analysis of all available surface in-situ, airborne and satellite observations (CIS 2009). The U.S. National Snow and Ice Data Center (NSIDC) in collaboration with the U.S. National Ice Center also generate daily sea ice extent product over the Northern Hemisphere in map form termed the Multi-sensor Analyzed Sea Ice Extent - Northern Hemisphere (MASIE-NH) (Fetterer et al. 2010). The MASIE product at 1-km spatial resolution is available since December 2014 from the NSIDC data archive (ftp://sidads.colorado.edu/DATASETS/NOAA/G02186/geotiff/1km/ice_only/).

Once the landfast ice is formed, its general dynamics are mostly controlled by thermodynamic factors (Barry et al. 1979), although the outer seaward ice edge can be affected by the ocean and atmospheric circulation (Carmack and Chapman 2003). Polyakov et al. (2012) reported a reduction of landfast ice thickness in the eastern Arctic associated with long-term trends in atmospheric thermodynamics. Howell et al. (2016) reported the trends of landfast ice thickness for the 1957–2014 period from local site observations. The trends were statistically significant at Cambridge Bay (-4.31 ± 1.4 cm decade^{-1}), Eureka (-4.65 ± 1.7 cm decade^{-1}) and Alert (-4.44 ± 1.6 cm decade^{-1}), although the data at Resolute did not show a statistically significant trend. The authors also observed that snow depth is associated more strongly with landfast ice thickness, while ice thickness and temperature demonstrated a somewhat lower correlation.

Galley et al. (2012) analyzed the timing of landfast sea ice conditions in the Canadian Arctic for the 1983–2009 period using the ice charts produced by the Canadian Ice Service. The CIS data in Galley et al. (2012) study were rasterized to a 2×2 km grid. Galley et al. (2012) identified the landfast ice as grid cells with the total sea-ice concentration coded as $10/10^{ths}$ referring to Melling (2002) and Tivy et al. (2011). This approach can be considered as a somewhat simplified solution for the rasterization of the CIS ice charts because the landfast ice is defined as coastal ice

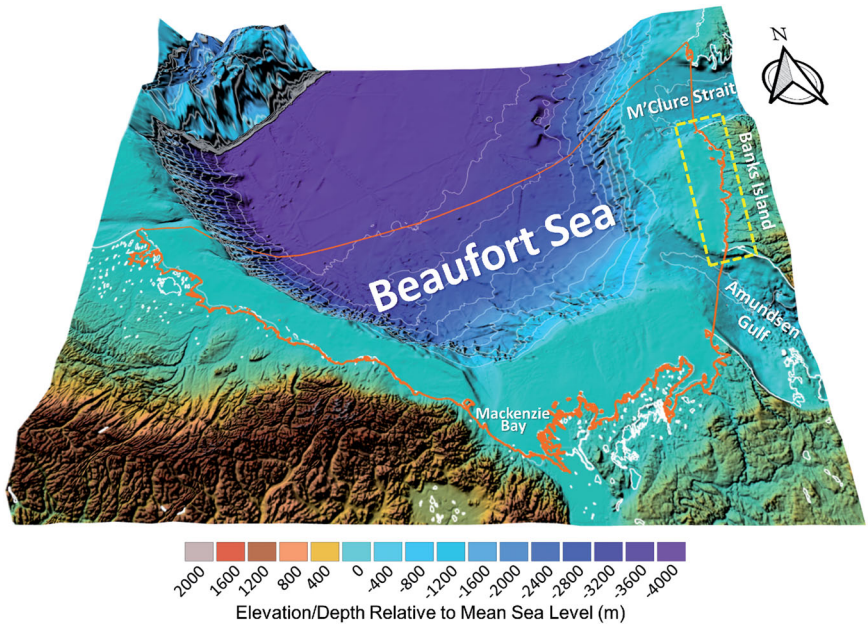

Figure 2. The surface elevation and bathymetry of the Beaufort Sea area (GEBCO Compilation Group 2020). The orange color line depicts the boundary of the Beaufort Sea projected on the seafloor, the features in white depict coastlines and inland water bodies, and the gray contours are isobaths.

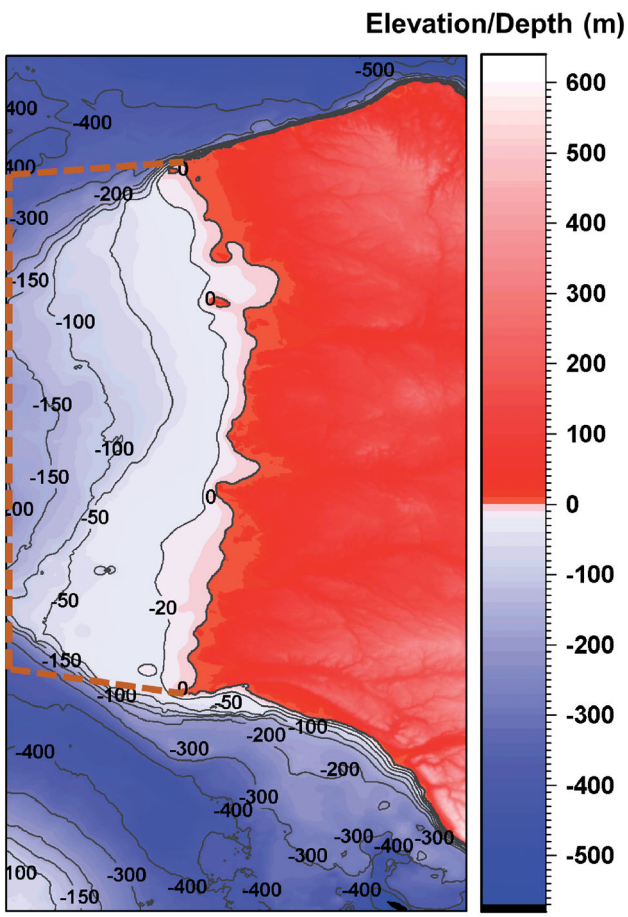

Figure 3. Map of the ocean floor bathymetry and surface elevation for the west coast of Banks Island. Data are obtained from the general bathymetric chart of the oceans (GEBCO Compilation Group 2020). Dashed lines denote the ocean zone utilized for the landfast ice analysis as shown in Figure 1b.

anchored to the land. As such, the property $10/10^{\text{ths}}$ may be a necessary condition, but it is not a sufficient condition for the ice to be classified as landfast ice. Galley et al. (2012) observed the earlier breakup and later onset dates and a general reduction of landfast ice duration in many areas of the Canadian Arctic region over the period analyzed. They reported the following non-significant trends for Banks Island: onset rate of change is 0.97 weeks/decade (later) with $p = 0.44$ and breakup rate of change is -1.17 weeks/decade (earlier) with $p = 0.14$, where p-value denotes the statistical significance of the trend.

Yu et al. (2014) analyzed the U.S. National Ice Center's weekly sea ice charts to study the variations of landfast ice extent from 1976 to 2007. The ice charts data were digitally rasterized to the Equal-Area Scalable Earth Grid (EASE-Grid) format at 25-km spatial resolution (Brodzik and Knowles 2002). The winter (January to May) mean extent of landfast ice for the entire Beaufort Sea region was found to be $50.04 \times 10^3\,\text{km}^2$, with a negative trend $-0.39 \pm 0.16 \times 10^3\,\text{km}^2\,\text{yr}^{-1}$ or $-7.79 \pm 3.20\%\text{decade}^{-1}$ in the relative annual mean area over the 1976–2007 period. This is close to the magnitude $-6.67 \pm 1.48\%\text{decade}^{-1}$ of the relative trend in annual mean area for the entire Northern hemisphere. Another example of coarse resolution landfast ice analysis is the study of the north-eastern part of the Kara Sea over the 1953–1990 period conducted by Divine et al. (2003). They utilized a grid with a spatial

resolution of 12.5 km to rasterize the ice charts produced by the Arctic and Antarctic Research Institute (AARI), in St. Petersburg, Russia (Borodachev 1998) with a temporal frequency that varied initially from one chart per month to three per month in later years. The authors reported a general trend indicating a reduction of landfast ice in this region.

The general requirement for spatial resolution of sea ice extent/edge defined by the Global Climate Observing System (GCOS) is 1–5 km (GCOS 2016). As such, the spatial resolution of 25 km and 12.5 km may be considered somewhat coarse for detailed local studies of landfast ice. It would be interesting to use higher resolution data for revisiting the LFI analysis for the regions where the edge of landfast ice is located close to the shore. These types of analyses can be conducted using high-resolution Synthetic Aperture Radar (SAR) and optical/thermal imagery.

Dammann et al. (2019) used Sentinel-1 interferometry (C-band SAR) to map the pan-Arctic landfast sea ice in 2017 at a spatial resolution of approximately 23×28 m. They utilized image pairs with a temporal lag of 12 or 24 days to map three categories of coastal ice: (a) bottomfast ice, (b) stabilized floating landfast ice, (c) nonstabilized floating coastal ice. This study emphasized several important points: (1) landfast ice mapping benefits from high-resolution imagery, (2) the method with interferograms obtained over intervals of a few weeks can provide more accurate information about landfast ice. It considers the dynamic stability rather than near-instantaneous images of the ice concentration as the latter may lack sufficient information related to ice stability at the highest concentration level $10/10^{ths}$. This approach still raises a question about the appropriate length of time interval to define the stability of landfast ice.

A comprehensive study of landfast ice in the Chukchi and Beaufort Seas has been conducted by Mahoney et al. (2014) using high-resolution SAR imagery spanning the period 1996–2008. The Beaufort Sea region considered in their study included only the western part stretching from the boundary with the Chukchi Sea in Alaska to Mackenzie Bay. The areas to the East of Mackenzie Bay including Banks Island were not covered. The authors detected positive trends (later dates) in the timing of landfast ice setup and negative trends (earlier dates) in the timing of breakup and ice-free conditions, i.e., shorter duration of landfast ice presence between 1996 and 2008. Integrating their previous studies of the same region (Mahoney, Eicken, et al. 2007; Mahoney, Eicken, Shapiro 2007), they reported that the mean width of the landfast ice zone in the western part of the Beaufort Sea in April is about 31 km, and in the Chukchi Sea it is 14 km. As such, the application of 25-km and even 12.5-km spatial resolution data for landfast ice studies in these regions is highly questionable.

Comparing results from Yu et al. (2014), Dammann et al. (2019) and Li et al. (2019) for the Beaufort Sea one can see some important differences reported for the LFI extent. For example, Dammann et al. (2019) reported the LFI extent (bottomfast, stabilized and non-stabilized) over the Beaufort Sea between March and May 2017 equal to 67×10^3 km^2. Yu et al. (2014) reported the average value of 50.04×10^3 km^2 for January-May over the 1976–2007 interval. Li et al. (2019) did not include numerical results for the landfast ice extent, as they showed only graphical materials. Figure 5 in Li et al. (2019) shows the 1976–2018 annual mean landfast ice extent over the Beaufort Sea that varied approximately in the range of $(25–40) \times 10^3$ km^2 with a mean value approximately equal to $(30–35) \times 10^3$ km^2 and the 2017 extent approximately equal to 30×10^3 km^2. The values reported above correspond to different averaging intervals and were derived from data with a spatial resolution that varies greatly between data sets. Consolidation and verification of these results require the development of new alternative approaches and is one of the goals of our study.

The main objectives of this study are threefold: (1) to study the applicability of the clear-sky composite products generated from MODIS data at CCRS at 250-m spatial resolution with 10-day intervals for delineation of landfast ice in the Canadian Arctic region; (2) to analyze how our landfast ice mapping results compare with the CIS ice charts and other sources; (3) to analyze trends in various landfast ice parameters since 2000 for the western coast of Banks Island facing the Beaufort Sea. This paper reports the results of our pilot study over the western coastline of Banks Island before expanding this approach to the entire area of the Beaufort Sea. The landfast ice along the western coastline of Banks Island represents a relatively simple case in comparison to other coastal zones of the Beaufort Sea (Environment Canada 2015).

CCRS MODIS composites and landfast ice delineation

The Moderate Resolution Imaging Spectroradiometer, or MODIS, operated by NASA is one of the most

advanced sensors presently utilized for a wide range of land, ocean and atmosphere applications (Salomonson et al. 1989). The instrument includes thirty six spectral bands with spatial resolution varying from 250 m to 1 km at nadir. The MODIS bands B1 and B2 are available at 250 m spatial resolution, additional five solar bands designed for land applications (B3 to B7) are available at 500 m spatial resolution. The remaining 29 bands have 1 km spatial resolution in the nadir direction. Two MODIS instruments are currently operational: (1) MODIS on the TERRA satellite and (2) MODIS on the AQUA satellite. Regular MODIS observations began in early 2000 and continue to the present time with daily measurements over the globe.

The clear-sky composite products over Canada are produced for MODIS bands B1-B7 at CCRS from the original Level 1B MODIS swath data distributed via the NASA DAAC Earth Observing System Data Gateway (https://ladsweb.modaps.eosdis.nasa.gov/). The MODIS 500-m land bands (B3-B7) are downscaled to 250 m spatial resolution compatible with bands B1 and B2 using adaptive regression and normalization scheme, as described in Trishchenko et al. (2006). Then, all data are re-projected into the required map projection using software also developed at CCRS (Khlopenkov and Trishchenko 2008). The re-projected images are composited as 10-day (3 per month, 36 per year) clear-sky products for Canada and the Northern Circumpolar area using a clear-sky, cloud and cloud shadow detection technique developed at CCRS (Luo et al. 2008, Trishchenko et al. 2009). Only the data from the MODIS sensor on the TERRA satellite are regularly processed at CCRS because the MODIS sensor on the AQUA satellite suffers from substantial band-to-band misalignment and a significant number of dead detectors (Khlopenkov and Trishchenko 2008; Xiong et al. 2005, 2006). Clear-sky composites are produced separately for the backward (i.e., sun-satellite relative azimuth angle range -90° to $+90^\circ$) and the forward (sun-satellite relative azimuth angle range 90° to 270°) scattering directions to account for surface bidirectional properties (Luo et al. 2008).

The main intended use of the CCRS clear-sky composites is for land applications (Beaudoin et al. 2014; Bernier et al. 2011; Betts et al. 2014, 2019; Colditz et al. 2012, 2014; Fontana et al. 2010; Hanesiak et al. 2011; Ji et al. 2010; Liu et al. 2021; Trishchenko et al. 2009; Trishchenko, Leblanc, et al. 2016; Trishchenko and Wang 2018; Way and Lewkowicz 2016). The CCRS MODIS processing system has also been successfully applied to lake water quality and algal bloom mapping (El-Alem et al. 2012, 2014, 2019; Ratté-Fortin et al. 2018, 2020), lake ice mapping (Gignac et al. 2017) and several other applications (Oreopoulos et al. 2011; Wilson and Oreopoulos 2013).

An important high-level product derived from the CCRS MODIS time series is the warm season (April-September) snow/ice probability maps designed to study the annual dynamics of Minimum Snow/Ice (MSI) extent (Trishchenko, Leblanc, et al. 2016; Trishchenko 2020, Trishchenko and Ungureanu 2021). These time series are available at 250-m spatial resolution since 2000 for two regions: (a) Canada with neighboring landmass area, 5,700 km $\times$ 4,800 km, (b) the Northern Circumpolar area, 9,000 km $\times$ 9,000 km. Trishchenko and Wang (2018) demonstrated that MSI extent variations over the Canadian Arctic region derived from CCRS warm season snow/ice probability maps are very well correlated to variations in the local climate dynamics such as average temperature, energy fluxes, and snow cover. The 20-year sequence of these snow/ice probability maps over the western marine coastal zone of Banks Island is displayed in Figure 4. The distinct feature of these maps is the systematically increased probability of sea ice occurrence along the western coastline of Banks Island. For most years, this coastline zone is separated from the icy waters in the central Beaufort Sea area by a transition zone with much lower values of probability of sea ice occurrence. Despite the clear visual indication of landfast ice, it is not a simple procedure to prove that this is landfast ice and to derive its main parameters, such as the total extent, linear dimensions, and temporal dynamics, as we deal with seasonally-aggregated probability products. As such, these probability maps may serve mainly as qualitative characteristics of sea ice conditions in the coastal zone.

We utilized 10-day 250-m MODIS image clear-sky composites for both directions (forward and backward scattering) aggregated to monthly intervals for a detailed quantitative analysis of the coastal sea ice dynamics and landfast ice identification. The mean (m) and standard deviation (σ) values of spectral reflectances for MODIS bands B1 (red), B2 (near-infrared), B4 (green), and B6 (shortwave infrared) have been derived for each month. Examples of such monthly maps for May 2013 are shown in Figures 5a and 5b. Panel (a) shows the false-color image derived from monthly mean reflectances for MODIS bands B6, B2 and B1 combined as RGB layers, and panel (b) shows the false-color image derived from standard

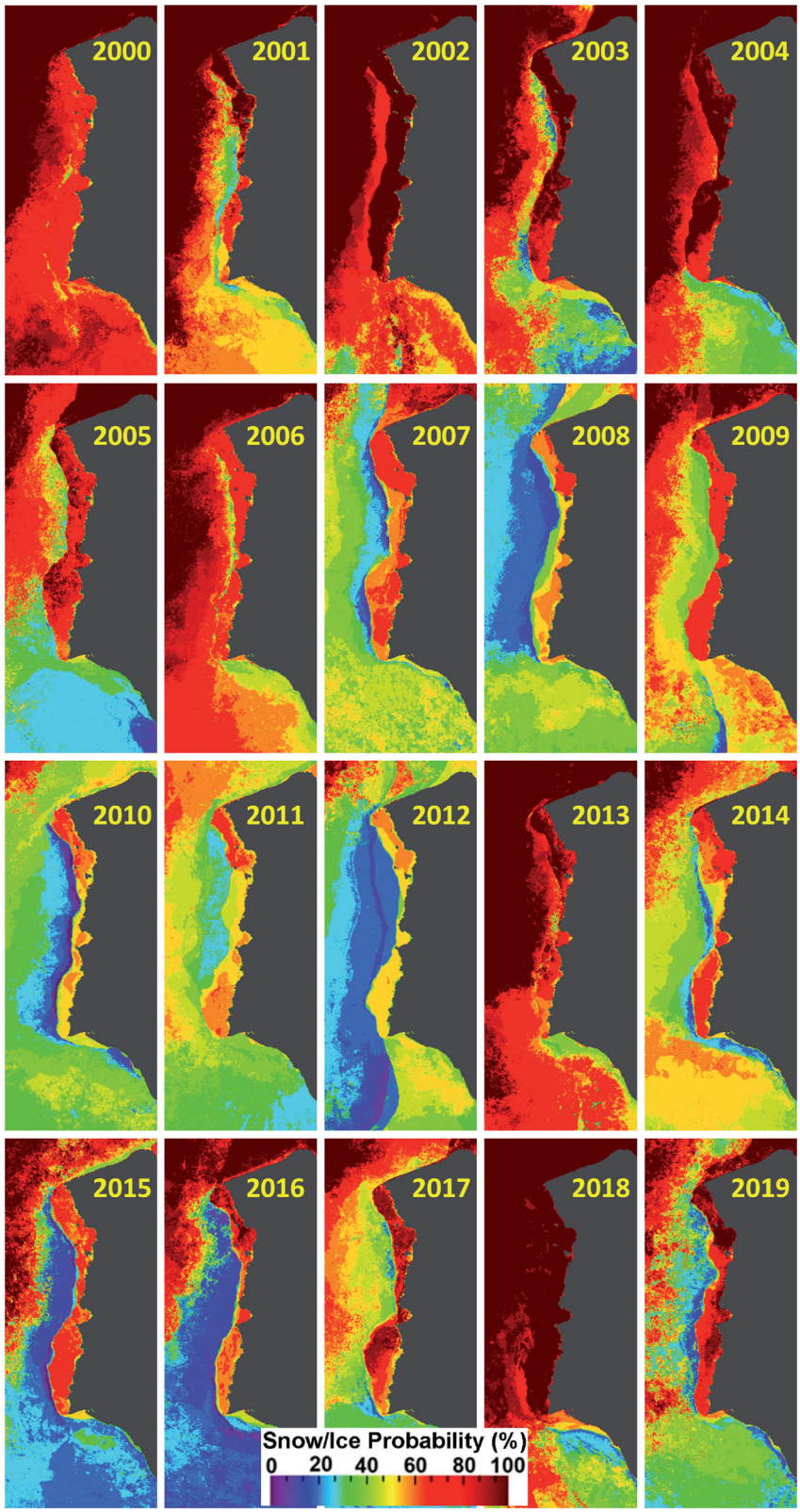

Figure 4. The 20-year sequence of melting season (April-September) snow/ice probability maps over the study region around Banks Island for 2000–2019.

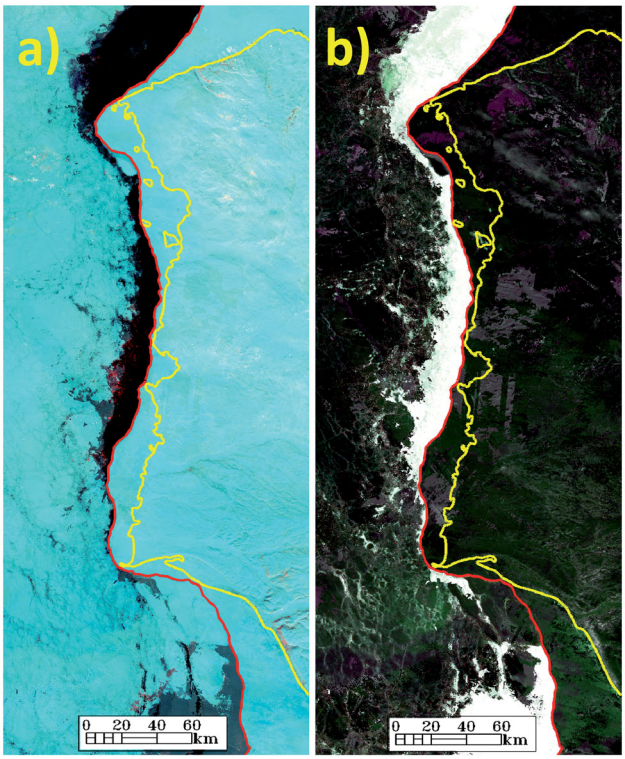

Figure 5. The average and standard deviation maps for the coastal zone with landfast ice. MODIS monthly data for May 2013. (a) False-color image from monthly average reflectances (RGB: B6, B2, B1); (b) false-color image from monthly standard deviations (RGB: B4, B2, B1). The red line denotes the boundary of landfast ice, the yellow line denotes the coastline of Banks Island and small islands in the vicinity.

deviations of reflectances for MODIS bands B4, B2, B1 combined as RGB layers. The composite maps from the mean reflectances can be used to identify the areas of sea ice, as MODIS bands B1, B2, and B6 have a very high potential for separating water bodies and snow-free land from snow/ice-covered surfaces. The monthly maps of standard deviations for bands B1, B2, and B4 serve for the identification of variability in spectral reflectances. The areas of high σ-values point to unstable sea ice conditions because spectral reflectances of water and sea ice differ greatly. The areas of low σ-values indicate persistently similar surface reflectance values during the entire month and, therefore, point to stable sea ice or open water conditions. These two maps have to be analyzed jointly.

Initially, we attempted to develop and implement an automated detection scheme. The automated approach did not lead to unambiguous results and required significant manual effort to remove the noise and residual cloud contamination in the input data. Some approaches for automated identification of landfast zone and associated difficulties have been discussed in Dammann et al. (2019), Meyer et al. (2011), Fraser et al. (2010), and references therein. The automated LFI identification may include several steps that combine various pattern recognition methods with morphological (median, erosion, and dilation) filters, patch size analysis, image differencing or other change detection techniques, to delineate areas of stabilized and non-stabilized LFI. Due to inconsistent results from the automated approach, we mapped the landfast zones manually and subjectively, employing the visual contrasts in two images (m and σ). Examples of such manual delineation of the landfast ice are displayed in Figures 5a and 5b by the red curves. Because the CCRS MODIS clear-sky composites contain spectral bands B1-B7 in the solar spectral domain, the quality of images in the high Arctic zone during the winter season (October–March) is low due to small sun elevation angles. As such, the period of LFI data extracted from CCRS MODIS clear-sky composites was limited to the April–September time frame. The CCRS LFI data are available at this link ftp://ftp.ccrs.nrcan.gc.ca/ad/Trishchenko/BeaufortSea LandfastIce.2000-2019/.

Landfast ice from Canadian Ice Service charts

The CIS ice charts are produced manually by experienced ice analysts on a regular basis (e.g., daily and weekly depending on areas and seasons). The ice features are validated for a specific time by analyzing and integrating all the data acquired for that time, including satellite observations, aerial surveys, and in-situ surveillance, as well as data from the weather forecast model. The Canadian Ice Service charts have been rasterized in this study from the vector data stored in the ArcInfo E00 file format (https://iceweb1.cis.ec.gc.ca/Archive/). The vector data are generated using a map scale up to 1:400,000, which theoretically could correspond to a raster pixel resolution of about 200 m. The coding of parameters in E00 files follows recommendations of the Sea Ice Geo-Referenced Information and Data (SIGRID) standard (JCOMM 2014). For mapping the landfast ice we utilized the "**form of ice**" codes (F#, where # could be A, B, C, etc. for different ice thickness situations). The landfast ice is coded by value 08 in any of the form of ice fields FA, FB, FC, etc. This method is different from the one selected by Galley et al. (2012) who utilized the "**ice concentration**" codes (C#), i.e., CT, CA, CB, etc. The SIGRID format uses code 92 for $10/10^{ths}$ ice concentration (JCOMM 2014). There are no formal recommendations in SIGRID to link the landfast ice to the ice concentration, although the landfast ice is

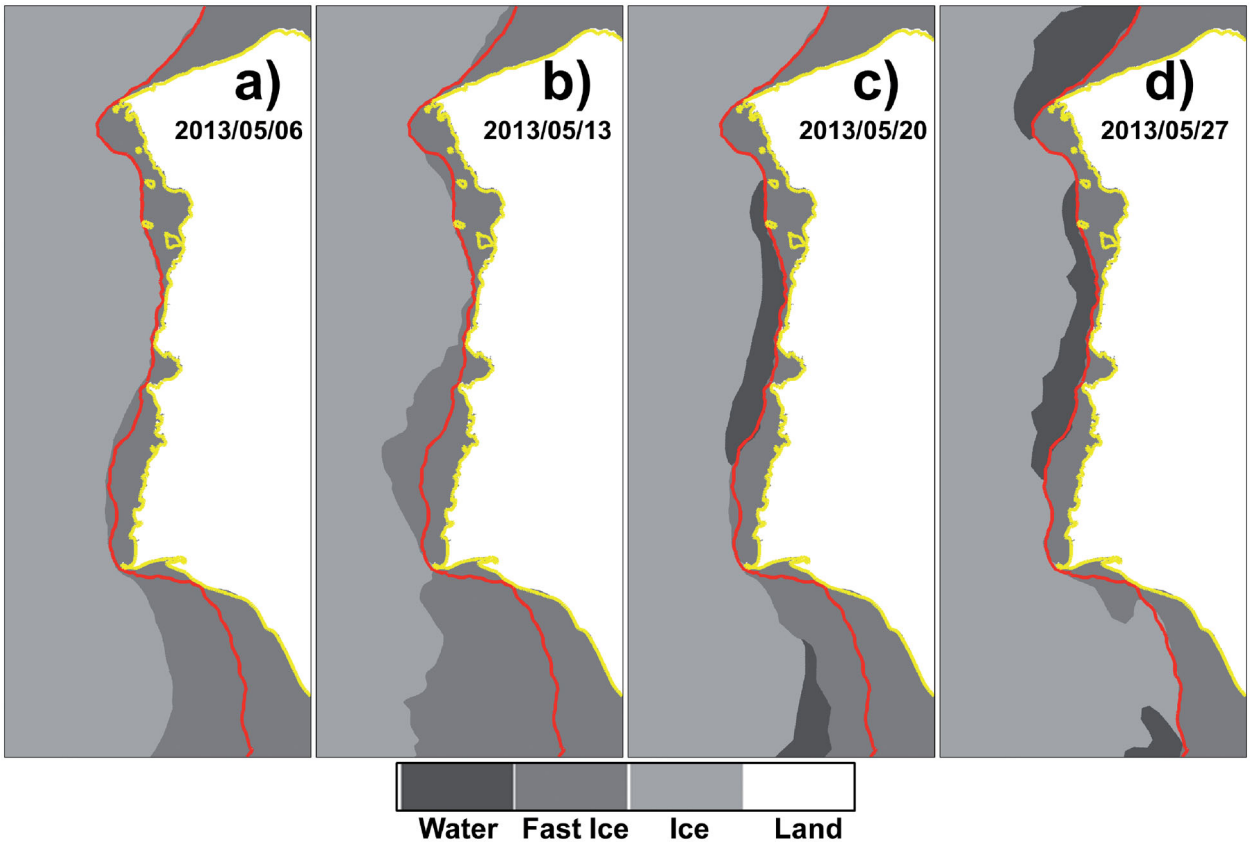

Figure 6. Examples of rasterized CIS ice charts (gray-coloured areas) for the Banks Island study region in May 2013. Red and yellow lines denote CCRS landfast delineation for this month (Figure 5), and coastline, respectively. Dates of the CIS ice chart are shown in each panel (a–d).

usually associated with the highest ice concentration code 92.

FORTRAN code has been written, as part of this study, to generate the raster data with 250-m spatial resolution in a map projection compatible with the CCRS MODIS clear-sky composites. Most of the CIS data files between 2000 and 2019 are available at weekly temporal resolution. Before 2008, some data for the January- April period may be available at monthly or semimonthly intervals. Each E00 file name contains a date coded as YYYYMMDD to represent the year, month, and day. This timestamp indicates the date for which the chart has been produced based on the best available input information collected from spaceborne, airborne, and in-situ observations for that date.

An example of rasterized CIS ice charts for the Banks Island region is shown in Figure 6 for May 2013. Four panels a-d show weekly maps of ice conditions. The rasterized maps display four classes: (1) open water, (2) landfast ice, (3) mobile ice in any concentration, form, and age, and (4) land. The CCRS delineation of landfast ice from Figure 5 is also shown here as a red line. Since it was derived from several clear-sky composite images over the one-month interval, it closely follows a minimum landfast ice line that could be expected from the four CIS ice maps. The visual inspection of results presented in Figure 6 allows us to make three preliminary conclusions: (1) the outer seaward edge of the landfast ice zone along the Banks Island mapped from the weekly CIS ice charts varies noticeably during a month; (2) the CCRS LFI zone derived from analysis of monthly data resembles closely the minimum landfast ice extent for the four-weekly composites, which indicates a possibility of high-concentration mobile ice mapped as landfast ice in CIS data; (3) the landfast ice identification in CIS ice chart may benefit from multi-temporal analysis of satellite imagery to detect the stabilized and non-stabilized (mobile) components of landfast ice.

Time series of raster files from CIS ice charts have been produced from January 2000 to the end of December 2019. Because of uneven temporal spacing (weekly, semimonthly and monthly) of CIS data, we replicated the low-frequency data points to a weekly

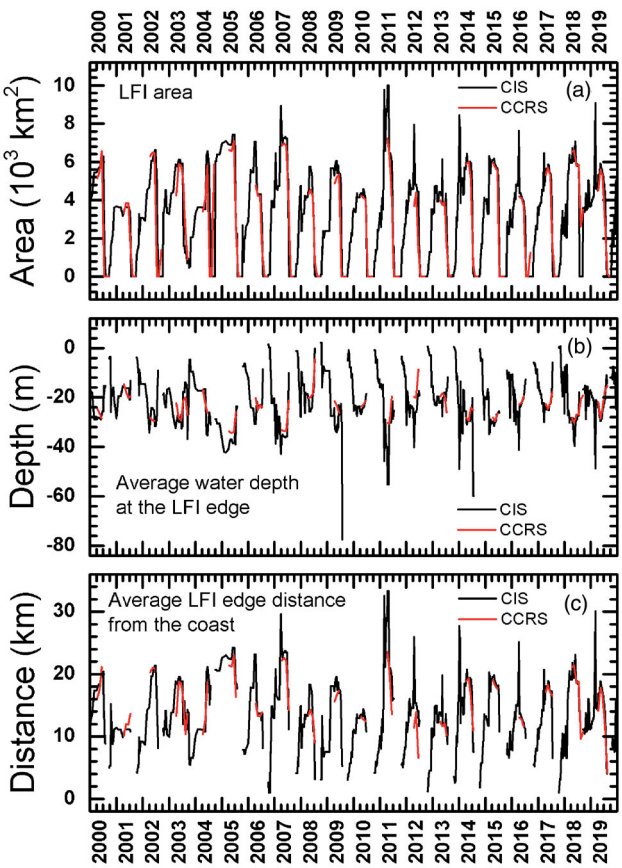

Figure 7. Time series of (a) LFI area, (b) the average water depth at the outer seaward LFI edge, (c) the average distance from the coast to the outer seaward LFI edge.

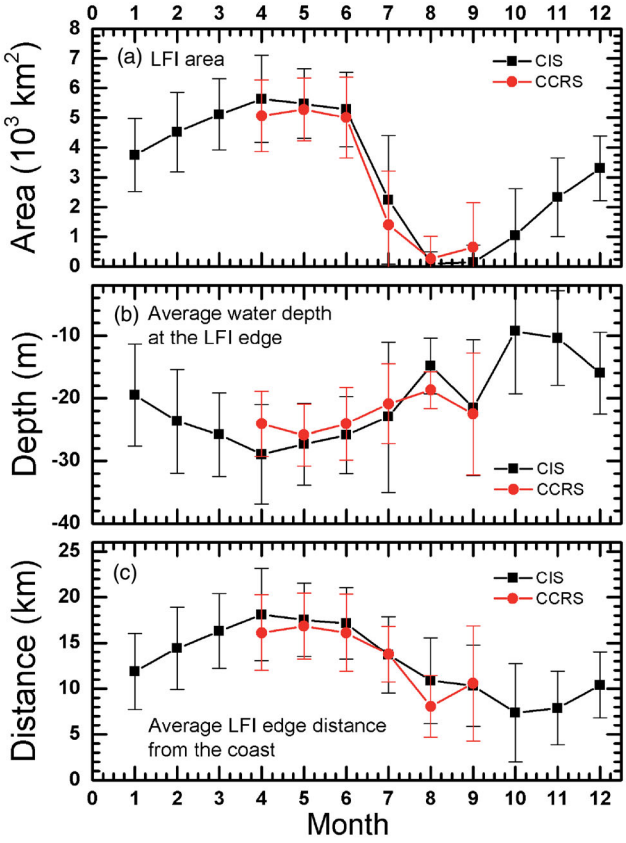

Figure 8. The monthly mean values averaged over 2000–2019 period. The corresponding standard deviations are plotted as error bars. Panels (a–c) as in Figure 7.

temporal resolution when computing monthly and seasonal statistics. This procedure ensures the proper weighting of observations and reduces possible biases due to unequal sampling.

Landfast ice statistics and trends for Banks Island

The following main parameters of the landfast ice have been determined for the Banks Island coastal zone in the Beaufort Sea confined by the dashed lines in Figure 3: (a) the LFI area, (b) the distance of outer seaward LFI edge from the coast, (c) the ocean depth at the outer seaward LFI edge, (d) the date of LFI onset, (e) the date of LFI break-up, (f) the length of the ice-free period (as a conjugate parameter to the landfast ice time duration). The timing parameters have been derived from the CIS time series, as the CCRS monthly data are of too coarse temporal resolution for this purpose. We utilized several threshold values for LFI area S to determine the ice-free intervals, the onset and break-up dates: (1) $S = 0\,km^2$; (2) $S = 500 km^2$; (3) $S = 1{,}000\,km^2$.

Table 1. Comparison of CIS and CCRS LFI monthly mean values for the total LFI area in the Banks Island coastal zone of the Beaufort Sea over 2000–2019.

Month	CIS (km^2)	CCRS (km^2)	Diff (km^2)
1	3,749 (1,228)	–	–
2	4,517 (1,338)	–	–
3	5,112 (1,195)	–	–
4	5,636 (1,465)	5,068 (1,202)	567
5	5,477 (1,164)	5,282 (1,056)	195
6	5,280 (1,250)	5,009 (1,362)	271
7	2,239 (2,156)	1,407 (1,803)	832
8	108 (385)	257 (764)	−149
9	142 (578)	648 (1,495)	−506
10	1,044 (1,579)	–	–
11	2,329 (1,327)	–	–
12	3,301 (1,090)	–	–
1–5	4,898	–	
4–6	5,464	5,120	344 or 6.3%

The standard deviations are given in parentheses.

Figure 7 shows the overall comparison of CIS and CCRS data for the entire period of 2000–2019 at the original temporal resolution. Three panels in Figure 7 display results for the total LFI area (a), the average ocean depth at the outer seaward edge of the LFI zone (b), the average distance of the outer seaward LFI edge from the coast (c). The CIS results are plotted in black. The CCRS results are plotted in red and restricted to the April-September period.

Table 2. The same as in Table 1 but for comparison of CIS and CCRS LFI monthly mean values for the average ocean depth at the outer seaward LFI edge.

Month	CIS (m)	CCRS (m)	Diff (m)
1	−19.5 (8.1)	–	–
2	−23.7 (8.3)	–	–
3	−25.8 (6.7)	–	–
4	−29.0 (7.9)	−24.1 5.2()	−4.9
5	−27.3 (6.5)	−25.9 (4.9)	−1.4
6	−25.9 (6.1)	−24.1 (5.8)	−1.8
7	−23.0 (11.9)	−20.9 (6.4)	−2.1
8	−14.8 (4.4)	−18.7 (2.9)	+3.9
9	−21.5 (10.8)	−22.5 (9.7)	+1.0
10	−9.3 10.0()	–	–
11	−10.4 (7.6)	–	–
12	−16.0 (6.5)	–	–
1–5	−25.1	–	
4–6	−27.4	−24.7	−2.7

Table 3. The same as in Table 1 but for the average distance of the outer seaward LFI edge from the coast.

Month	CIS (km)	CCRS (km)	Diff (km)
1	11.9 (4.1)	–	–
2	14.4 (4.5)	–	–
3	16.3 (4.1)	–	–
4	18.1 (5.1)	16.1 (4.1)	2.0
5	17.5 (4.0)	16.8 (3.6)	0.7
6	17.1 (3.9)	16.1 (4.2)	1.0
7	13.7 (4.2)	13.8 (3.0)	−0.1
8	10.9 (4.7)	8.1 (3.4)	2.8
9	10.3 (4.4)	10.6 (6.3)	−0.3
10	7.46 (5.3)	–	–
11	7.9 (4.0)	–	–
12	10.4 (3.6)	–	–
1–5	15.6	–	
4–6	17.6	16.3	1.3

The data show a high degree of consistency. One can also notice relatively higher variability of the CIS results relative to the CCRS time series. We attribute this to the possible inclusion of variable mobile ice at the outer ice edge in the landfast ice field in the CIS ice charts because they are produced from the data collected on a specific date, unlike the monthly time scale aggregation employed in the CCRS method.

The mean seasonal cycle over the 20-year period for the total area, the average distance from the coast, and the mean ocean depth at the outer seaward LFI edge are plotted in Figures 8a, 8b, and 8c. The numbers are provided in Table 1 for the LFI area, Table 2 for the ocean depth, and Table 3 for the distance. Tables include the mean values and standard deviations for each month, as well as statistics computed for January-May and April-June intervals. The differences between comparable data are also included. Results presented in Figure 8 and Tables 1–3 show that LFI in the Bank Island zone reaches maximum spatial extent in April according to CIS data (5,636 km^2), while for CCRS data it reaches a maximum in May (5,282 km^2). Both datasets show that April, May, and June have the three largest values of

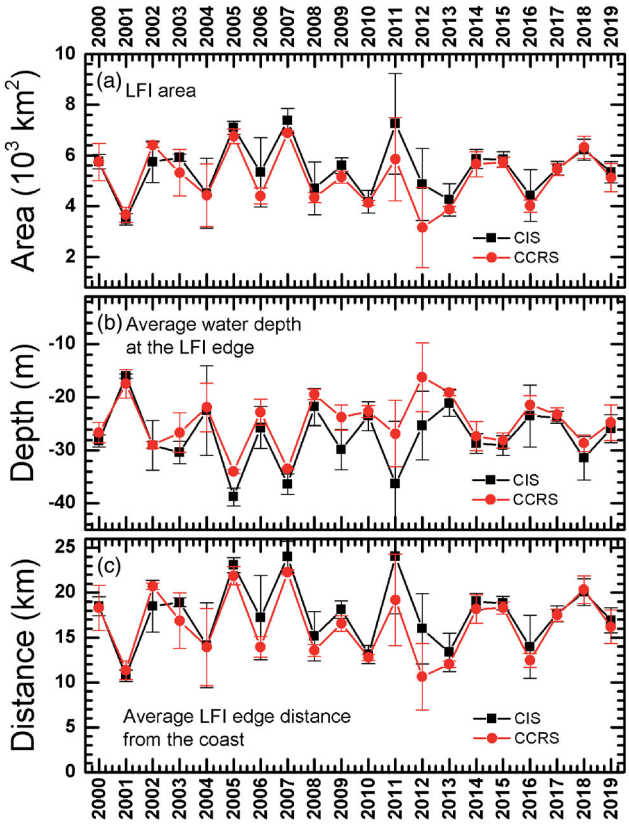

Figure 9. Multi-year time series of the April–June mean values. Panels (a–c) as in Figures 7 and 8.

the LFI total area. The CCRS data are smaller than the CIS data in most cases except for September. However, the data for September are at the low end of the scale and highly variable. The systematic underestimation of the total LFI area in CCRS data relative to the CIS results serves as an indication of a different treatment of mobile ice at high concentration in these two approaches, as discussed above. This is also consistent with the data shown in Figures 8b and 8c for the LFI edge. The mean distance of the outer seaward LFI edge is generally closer to the shore in CCRS data and corresponds to more shallow waters. The August and September data for the depth demonstrate the opposite behavior, however, they are based on a reduced number of cases (3 and 6 points for CCRS and 8 and 9 points for the CIS dataset out of 20). The total LFI area is also quite small, which makes these results statistically less significant.

The multi-annual time series of aggregated values for the April-June period, which contains the three largest LFI monthly extent values in both datasets, are displayed in Figure 9 for the same parameters as in Figure 8. All results demonstrate a high degree of consistency. The correlation coefficients between CCRS and CIS data for the total LFI area and outer seaward

distance are equal to 0.88. The correlation coefficient for the depth is 0.87. The differences (CIS-CCRS) are 344 km^2 (5,464 km^2 vs 5,120 km^2) or 6.3% for the LFI spatial extent; 1.3 km (17.6 km vs 16.3 km) or 7.4% for the distance from the coast; −2.7 m (−27.4 m vs −24.7 m) or 10% for water depth at the LFI outer edge.

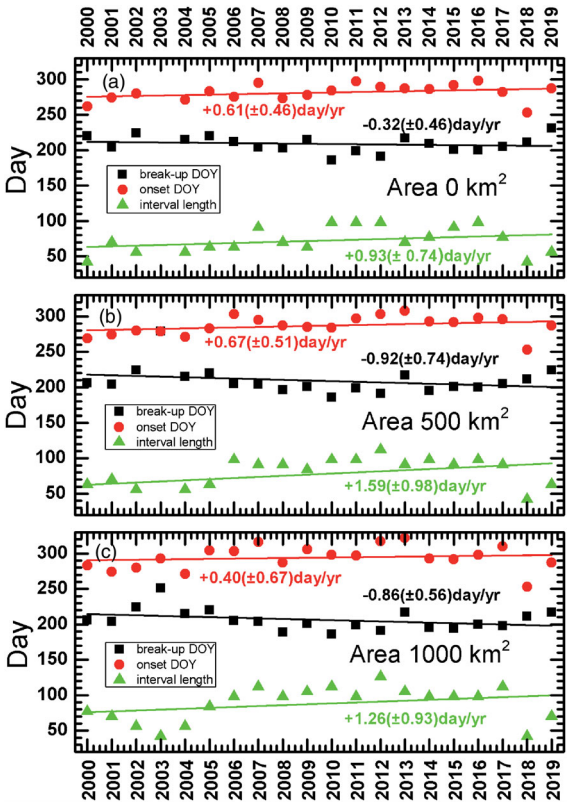

Figure 10. Trends in a break-up, onset and LFI off-season duration for various thresholds in the total LFI area. (a) 0 km^2; (b) 500 km^2; (c) 1,000 km^2. Lines denote the linear trends. Numbers show the absolute values and their errors. The break-up dates are displayed in black, onset dates are displayed in red, the length of LFI off season is shown in green. None of the displayed trends is statistically significant.

The distance of the outer edge of landfast ice from the coast describes the width of the landfast ice zone. It is evident from our results that adequate analysis of phenomena with a typical size under 20 km is not possible using data with spatial grid cells of 25 km (Yu et al. 2014; Li et al. 2019).

The long-term trends since 2000 in the dates of LFI onset, break-up and the length of an ice-free interval are shown in Figure 10 and are also reported in Table 4. The average Day-Of-Year (DOY) values, DOY standard deviations, the estimates of trends and their uncertainties are provided. Results demonstrate the tendency for an earlier break-up, later onset and longer ice-free period, however, these trends are not statistically significant. The p-values (Prob>$|t|$) vary from 0.12 to 0.56, which is much larger than the value 0.05 typically assumed for statistically significant results. These results are generally consistent with those reported by Galley et al. (2012) for the 1983–2009 period.

Discussion and conclusions

Despite a significant number of publications and a long history of research, some important uncertainties regarding the accuracy of landfast ice mapping in the Canadian Arctic still exist. In particular, the impact of potentially mobile ice at high concentration (10/10th) located at the outer edge of the coastal ice in operational ice charts has not been sufficiently quantified. Several recent case studies based on high-resolution SAR imagery revealed that accurate climatology of the landfast ice should be based on data with much higher spatial resolution than what was often utilized in previous studies (Yu et al. 2014; Li et al. 2019; Divine et al. 2003). Besides, no systematic validation efforts have been undertaken to derive the landfast ice maps using an independent and alternative approach over a multi-year period and to compare those results against

Table 4. The long-term trends of LFI seasonal cycle evolution in the Banks Island coastal zone of the Beaufort Sea derived from CIS ice charts for different thresholds of LFI extent.

Parameter	Mean (std) DOY	Trend (error) day/yr	p-Value Prob>$\|t\|$
Threshold LFI area S_0 = 0 km^2			
Break-up date	208.8 (11.3)	−0.32 (±0.46)	0.50
Onset date	281.4 (11.6)	+0.61 (±0.46)	0.20
Length of ice-off interval $S = S_0$	72.6 (18.7)	+0.93 (±0.74)	0.23
Threshold LFI area S_{500} = 500 km^2			
Break-up date	209.2 (19.5)	−0.92 (±0.75)	0.23
Onset date	286.9 (13.4)	+0.67 (±0.51)	0.20
Length of ice-off interval $S \leq S_{500}$	77.7 (26.3)	+1.59 (±0.98)	0.12
Threshold LFI area S_{1000} = 1,000 km^2			
Break-up date	206.4 (15.0)	−0.86 (±0.56)	0.14
Onset date	294.2 (16.9)	+0.40 (±0.67)	0.56
Length of ice-off interval $S \leq S_{1000}$	87.9 (24.5)	+1.26 (±0.93)	0.19

None of the trends is significant (i.e., $p > 0.05$).

operational ice charts. This study attempted to address some of these issues.

We developed the methodology for mapping the landfast ice using time series of 10-day clear-sky composites derived at the Canada Center for Remote Sensing (CCRS) from MODIS 250-m imagery. The method utilized the monthly mean and standard deviation of MODIS reflectance maps to manually delineate the landfast ice zone over the Banks Island coast in the Beaufort Sea. Monthly time series of landfast ice parameters for 20 years (2000–2019) have been produced. Due to solar zenith angle limitations, the method is restricted to the April-September period. Results have been utilized to evaluate their consistency with CIS ice charts. The comparison has demonstrated that the results from both methods are in good agreement. The average correlation coefficients between CCRS and CIS time series for landfast ice total area and the distance of outer seaward landfast ice edge from the coast in April–June, when the area reaches a maximum, are equal to 0.88. The correlation coefficient is 0.87 for the ocean depth at the outer seaward landfast ice edge. The relative differences varied between 6.3% and 10%. The long-term trends of the landfast ice season cycle in our region of interest since 2000 showed a tendency for an earlier break-up, later onset and longer ice-free period; however, these trends are not statistically significant.

Because the CCRS method uses monthly statistics, this approach tends to exclude potentially more mobile continuous landfast ice at the outer seaward edge zones than the CIS analysis, which is based on data collected on a specific date. Similar conclusions have been reported by Dammann et al. (2019) who utilized SAR image pairs with a temporal lag of 12 or 24 days. This explains a small (6.3% on average) underestimation of the LFI area from the CCRS method relative to CIS results. This finding highlights two important issues that still require further attention: (a) What is the length of optimal time interval for aggregating the input imagery and mapping the landfast ice; (b) How to combine the need for an extended data collection time interval with operational needs to produce timely and accurate ice charts that include many other categories describing the state of sea ice and ocean surface. Based on this study this optimal collection interval may vary from a few days to one month.

The width of the landfast ice zone for the Banks Island coast in the Beaufort Sea was found to be on average under 18.1(±5.1) km (the average value for April). As such, we recommend that the spatial resolution of landfast ice maps for adequate studies of climatology in this region should be at a sub-kilometre scale. From this point of view, the MODIS 250-m data and the Visible Infrared Imaging Radiometer Suite (VIIRS) 375-m satellite images (Murphy et al. 2006; Trishchenko 2019; Wolfe et al. 2013) suit landfast ice mapping in the Canadian Arctic very well; they are free and open access data sources that complement SAR imagery. The mapping of sea ice including landfast ice can benefit from the application of high-temporal resolution imagery from the satellite systems on Highly Elliptical Orbit (HEO) that allow continuous coverage of the polar region (Trishchenko and Garand 2011, 2012; Trishchenko et al. 2011; Trishchenko, Garand, et al. 2016; Trishchenko, Garand, et al. 2019; Trishchenko, Trichtchenko, et al. 2019).

Acknowledgments

This work was conducted as part of the Climate Change Geoscience Program and CCRS Long-Term Satellite Data Records (LTSDR) activity as part of the Cumulative Effects project at CCRS, Department of Natural Resources Canada (NRCan). The authors gratefully acknowledge the use of MODIS data acquired from the NASA Distributed Archive Center. The authors are grateful to G. Choma (CCRS/NRCan) for the careful editing of the manuscript and S. Leblanc (CCRS/NRCan) for the translation of the abstract into French. The manuscript was assigned the NRCan contribution number 20200759.

ORCID

Alexander P. Trishchenko http://orcid.org/0000-0002-9003-3345
Yi Luo http://orcid.org/0000-0001-8740-1912

References

Barry, R.G., Moritz, R.E., and Rogers, J.C. 1979. "The fast ice regimes of the Beaufort and Chukchi Sea coasts." *Cold Regions Science and Technology*, Vol. 1(No. 2): pp. 129–152. doi:10.1016/0165-232X(79)90006-5.

Beaudoin, A., Bernier, P.Y., Guindon, L., Villemaire, P., Guo, X.J., Stinson, G., Bergeron, T., Magnussen, S., and Hall, R.J. 2014. "Mapping attributes of Canada's forests at moderate resolution through kNN and MODIS imagery." *Canadian Journal of Forest Research*, Vol. 44 (No. 5): pp. 521–532. doi:10.1139/cjfr-2013-0401.

Bernier, P.Y., Desjardins, R.L., Karimi-Zindashty, Y., Worth, D., Beaudoin, A., Luo, Y., and Wang, S. 2011. "Boreal lichen woodlands: A possible negative feedback to climate change in eastern North America." *Agricultural and Forest Meteorology*, Vol. 151(No. 4): pp. 521–528. doi:10.1016/j.agrformet.2010.12.013.

Betts, A., Chan, D.Z., and Desjardins, R.L. 2019. "Near-surface biases in ERA5 over the Canadian Prairies." *Frontiers in Environmental Science*, Vol. 7: pp. 7. doi:10.3389/fenvs.2019.00129.

Betts, A.K., Desjardins, R., Worth, D., and Wang, S., and Li, J. 2014. "Coupling of winter climate transitions to snow and clouds over the Prairies." *Journal of Geophysical Research: Atmospheres*, Vol. 119(No. 3): pp. 1118–1139. doi:10.1002/2013JD021168.

Borodachev, V.E. 1998. *L'dy Karskogo Morya. (Ice in the Kara Sea)*. St. Petersburg: Gidrometeoizdat. 184 pp.

Brodzik, M.J., and Knowles, K.W. 2002. "Chapter 5: EASE-Grid: A versatile set of equal-area projections and grids." In *Discrete Global Grids: A Web Book*, edited by Michael F. Goodchild. Santa Barbara, CA: National Center for Geographic Information & Analysis. https://escholarship.org/uc/item/9492q6sm.

Canadian Ice Service (CIS). 2009. "Manual of Ice (MANICE)." Environment and Climate Change Canada. Available from https://www.canada.ca/en/environment-climate-change/services/weather-manuals-documentation/manice-manual-of-ice.html. Accessed October 15, 2020.

Carmack, E.C., and Chapman, D.C. 2003. "Wind-driven shelf/basin exchange on an Arctic shelf: The joint roles of ice cover extent and shelf-break bathymetry." *Geophysical Research Letters*, Vol. 30(No. 14): pp. 1778. 4pp. doi:10.1029/2003GL017526.

Colditz, R.R., López Saldaña, G., Maeda, P., Espinoza, J.A., Tovar, C.M., Hernández, A.V., Benítez, C.Z., Cruz López, I., and Ressl, R. 2012. "Generation and analysis of the 2005 land cover map for Mexico using 250-m MODIS data." *Remote Sensing of Environment*, Vol. 123: pp. 541–552. doi:10.1016/j.rse.2012.04.021.

Colditz, R.R., Pouliot, D., Llamas, R.M., Homer, C., Ressl, R.A., Tovar, C.M., Hernández, A.V., and Richardson, K. 2014. "Detection of North American land cover change between 2005 and 2010 with 250m MODIS data." *Photogrammetric Engineering and Remote Sensing*, Vol. 80(No. 10): pp. 918–924.

Cooley, S.W., Ryan, J.C., Smith, L.C., Horvat, C., Pearson, B., Dale, B., and Lynch, A.H. 2020. "Coldest Canadian Arctic communities face greatest reductions in shorefast sea ice." *Nature Climate Change*, Vol. 10(No. 6): pp. 533–538. doi:10.1038/s41558-020-0757-5.

Dammann, D.O., Eriksson, L.E., Mahoney, A.R., Eicken, H., and Meyer, F.J. 2019. "Mapping pan-Arctic landfast sea ice stability using Sentinel-1 interferometry." *The Cryosphere*, Vol. 13(No. 2): pp. 557–577. doi:10.5194/tc-13-557-2019.

Divine, D., Korsnes, R., and Makshtas, A. 2003. "Variability and climate sensitivity of land-fast ice extent in the North-Eastern Kara Sea." *Polar Research*, Vol. 22(No. 1): pp. 27–34. doi:10.3402/polar.v22i1.6440.

El-Alem, A., Chokmani, K., Laurion, I., and El-Adlouni, S.E. 2012. "Comparative analysis of four models to estimate chlorophyll-a concentration in case-2 waters using MODerate Resolution Imaging Spectroradiometer (MODIS) imagery." *Remote Sensing*, Vol. 4(No. 8): pp. 2373–2400. doi:10.3390/rs4082373.

El-Alem, A., Chokmani, K., Laurion, I., and El-Adlouni, S.E. 2014. "An adaptive model to monitor chlorophyll-a in inland waters in southern Quebec using downscaled MODIS imagery." *Remote Sensing*, Vol. 6(No. 7): pp. 6446–6471. Vol pp doi:10.3390/rs6076446.

El-Alem, A., Chokmani, K., Laurion, I., El-Adlouni, S.E., Raymond, S., and Ratte-Fortin, C. 2019. "Ensemble-based systems to monitor algal bloom with remote sensing." *IEEE Transactions on Geoscience and Remote Sensing*, Vol. 57(No. 10): pp. 7955–7971. doi:10.1109/TGRS.2019.2917636.

Environment Canada. 2015. *Beaufort Regional Coastal Sensitivity Atlas*. Ottawa: Environment Canada. 387 p.

Fetterer, F., Savoie, M., Helfrich, S., and Clemente-Colón, P. 2010. "Multisensor analyzed sea ice extent - Northern Hemisphere (MASIE-NH)." 1-km resolution ice product. Boulder, Colorado USA. NSIDC: National Snow and Ice Data Center. doi:10.7265/N5GT5K3K. Accessed November 9, 2020.

Flanders Marine Institute 2019. "Maritime boundaries geodatabase: Maritime boundaries and exclusive economic zones (200NM), version 11." Available online at http://www.marineregions.org/. doi:10.14284/386.

Fontana, F.M.A., Trishchenko, A.P., Luo, Y., Khlopenkov, K.V., Nussbaumer, S.U., and Wunderle, S. 2010. "Perennial snow and ice variations (2000-2008) in the Arctic circumpolar land area from satellite observations." *Journal of Geophysical Research*, Vol. 115(No. F4): pp. F04020. doi:10.1029/2010JF001664.

Fraser, A.D., Massom, R.A., and Michael, K.J. 2010. "Generation of high-resolution east Antarctic landfast sea-ice maps from cloudfree MODIS satellite composite imagery." *Remote Sensing of Environment*, Vol. 114(No. 12): pp. 2888–2896. doi:10.1016/j.rse.2010.07.006.

Fraser, R.H., Kokelj, S.V., Lantz, T.C., McFarlane-Winchester, M., Olthof, I., and Lacelle, D. 2018. "Climate sensitivity of high Arctic permafrost terrain demonstrated by widespread ice-wedge thermokarst on Banks Island." *Remote Sensing*, Vol. 10(No. 6):954; pp. 954. doi:10.3390/rs10060954.

French, H.M. 2016. "The tundra and polar semi-desert landscapes of Banks Island and Prince Patrick Island, western Canadian Arctic." *Cuadernos de Investigacion Geografica*, Vol. 42(No. 2): pp. 321–340. doi:10.18172/cig.2872.

Galley, R.J., Else, B.G.T., Howell, S.E.L., Lukovich, J.V., and Barber, D.G. 2012. "Landfast sea ice conditions in the Canadian Arctic: 1983-2009." *ARCTIC*, Vol. 65(No. 2): pp. 133–144. doi:10.14430/arctic4195.

GEBCO Compilation Group. 2020. "The general bathymetric chart of the oceans (GEBCO)." GEBCO 2020 Grid. doi:10.5285/a29c5465-b138-234d-e053-6c86abc040b9.

Gignac, C., Bernier, M., Chokmani, K., and Poulin, J. 2017. "IceMap250 - automatic 250-m sea ice extent mapping using MODIS data." *Remote Sensing*, Vol. 9(No. 1): pp. 70. 24pp. doi:10.3390/rs9010070.

Global Climate Observing System (GCOS). 2016." The global observing system for climate: Implementation needs. GCOS–200." 341 pp. https://library.wmo.int/index.php?lvl=notice_display&id=19838. Accessed September 25, 2020.

Hanesiak, J.M., Stewart, R.E., Bonsal, B.R., Harder, P., Lawford, R., Aider, R., Amiro, B.D., et al. 2011. "Characterization and summary of the 1999-2005 Canadian Prairie drought." *Atmosphere-Ocean*, Vol.

49(No. 4): pp. 421–452. doi:10.1080/07055900.2011.626757.

Howell, S.E.L., Laliberté, F., Kwok, R., Derksen, C., and King, J. 2016. "Landfast ice thickness in the Canadian Arctic Archipelago from observations and models." *The Cryosphere*, Vol. 10(No. 4): pp. 1463–1475. doi:10.5194/tc-10-1463-2016.

JCOMM. 2014. "SIGRID-3: A vector archive format for sea ice charts." Version 3.0; JCOMM Technical Report No. 23/WMO/Technical Document No. 1214; World Meteorological Organization, Geneva, Switzerland; May 2014. 40pp. Available at: https://www.jcomm.info/index.php?option=com_oe&task=viewDocumentRecord&docID=4439

Ji, L., Wylie, B., Ramachandran, B., and Jenkerson, C. 2010. "A comparative analysis of three different MODIS NDVI datasets for Alaska and adjacent Canada." *Canadian Journal of Remote Sensing*, Vol. 36(No. sup1): pp. S149–S167. doi:10.5589/m10-015.

Khlopenkov, K.V., and Trishchenko, A.P. 2008. "Implementation and evaluation of concurrent gradient search method for reprojection of MODIS level 1B imagery." *IEEE Transactions on Geoscience and Remote Sensing*, Vol. 46(No. 7): pp. 2016–2027. Vol doi:10.1109/TGRS.2008.916633.

Li, Z., Zhao, J., Su, J., Li, C., Cheng, B., Hui, F., Yang, Q., and Shi, L. 2019. "Spatial and temporal variations in the extent and thickness of Arctic landfast ice." *Remote Sensing*, Vol. 12(No. 1): pp. 64. doi:10.3390/rs12010064.

Liu, J., Worth, D.E., Desjardins, R.L., Haak, D., McConkey, B., and Cerkowniak, D. 2021. "Influence of two management practices in the Canadian Prairies on radiative forcing." *Science of the Total Environment*, Vol. 765: pp. 142701. doi:10.1016/j.scitotenv.2020.142701.

Luo, Y., Trishchenko, A.P., and Khlopenkov, K.V. 2008. "Developing clear-sky, cloud and cloud shadow mask for producing clear-sky composites at 250-meter spatial resolution for the seven MODIS land bands over Canada and North America." *Remote Sensing of Environment*, Vol. 112(No. 12): pp. 4167–4185. doi:10.1016/j.rse.2008.06.010.

Mahoney, A.R., Eicken, H., Gaylord, A.G., and Gens, R. 2014. "Landfast sea ice extent in the Chukchi and Beaufort Seas: The annual cycle and decadal variability." *Cold Regions Science and Technology*, Vol. 103 pp. 41–56. doi:10.1016/j.coldregions.2014.03.003.

Mahoney, A.R., Eicken, H., Gaylord, A.G., and Shapiro, L. 2007. "Alaska landfast sea ice: Links with bathymetry and atmospheric circulation." *Journal of Geophysical Research*, Vol. 112(No. C2): pp. C02001. doi:10.1029/2006JC003559.

Mahoney, A.R., Eicken, H., and Shapiro, L. 2007. "How fast is landfast sea ice? A study of the attachment and detachment of nearshore ice at Barrow, Alaska." *Cold Regions Science and Technology*, Vol. 47(No. 3): pp. 233–255. doi:10.1016/j.coldregions.2006.09.005.

Melling, H. 2002. "Sea ice of the northern Canadian Arctic Archipelago." *Journal of Geophysical Research*, Vol. 107(No. C11): pp. 3181. doi:10.1029/2001JC001102.

Meyer, F.J., Mahoney, A.R., Eicken, H., Denny, C.L., Druckenmiller, H.C., and Hendricks, S. 2011. "Mapping Arctic landfast ice extent using L-band synthetic aperture radar interferometry." *Remote Sensing of Environment*, Vol. 115(No. 12): pp. 3029–3043. doi:10.1016/j.rse.2011.06.006.

Murphy, R. P., Ardanuy, P. E., Deluccia, F., Clement, J. E., and Schueler, C. 2006. "The visible infrared imaging radiometer suite," In *Earth Science Satellite Remote Sensing*, edited by J.J. Qu, W. Gao, M. Kafatos, R.E. Murphy, and V.V. Salomonson, Vol. 1, 199–223. New York: Springer-Verlag.

Oreopoulos, L., Wilson, M.J., and Várnai, T. 2011. "Implementation on landsat data of a simple cloud-mask algorithm developed for MODIS land bands." *IEEE Geoscience and Remote Sensing Letters*, Vol. 8(No. 4): pp. 597–601. doi:10.1109/LGRS.2010.2095409.

Overland, J. E., Hanna, E., Hanssen-Bauer, I., Kim, S.-J., Walsh, J. E., Wang, M., Bhatt, U. S., Thoman, R. L., and Ballinger, T. J. 2019. "Surface air temperature." In *Arctic report card 2019*, edited by J. Richter-Menge, M. L. Druckenmiller, and M. Jeffries, 100. Washington, DC: NOAA. Available at https://arctic.noaa.gov/Report-Card/Report-Card-2019.

Polyakov, I.V., Walsh, J.E., and Kwok, R. 2012. "Recent changes of Arctic multiyear sea ice coverage and the likely causes." *Bulletin of the American Meteorological Society*, Vol. 93(No. 2): pp. 145–151. doi:10.1175/BAMS-D-11-00070.1.

Proshutinsky, A., Bourke, R.H., and McLaughlin, F.A. 2002. "The role of the Beaufort gyre in Arctic climate variability: Seasonal to decadal climate scales." *Geophysical Research Letters*, Vol. 29(No. 23): pp. 15-1–15-4. doi:10.1029/2002GL015847.

Ratté-Fortin, C., Chokmani, K., and El-Alem, A. 2018. "A novel algorithm of cloud detection for water quality studies using 250- m downscaled MODIS imagery." *International Journal of Remote Sensing*, Vol. 39(No. 19): pp. 6429–6439. doi:10.1080/01431161.2018.1460506.

Ratté-Fortin, C., Chokmani, K., and Laurion, I. 2020. "Spatiotemporal variability in phytoplankton bloom phenology in eastern Canadian lakes related to physiographic, morphologic, and climatic drivers." *Environments*, Vol. 7(No. 10): pp. 77. doi:10.3390/environments7100077.

Salomonson, V.V., Barnes, W.L., Maymon, P.W., Montgomery, H.E., and Ostrow, H. 1989. "MODIS: Advanced facility instrument for studies of the Earth as a system." *IEEE Transactions on Geoscience and Remote Sensing*, Vol. 27(No. 2): pp. 145–153. doi:10.1109/36.20292.

Tivy, A., Howell, S.E.L., Alt, B., McCourt, S., Chagnon, R., Crocker, G., Carrieres, T., and Yackel, J.J. 2011. "Trends and variability in summer sea ice cover in the Canadian Arctic based on the Canadian Ice Service digital archive, 1960 – 2008 and 1968 – 2008." *Journal of Geophysical Research*, Vol. 116(No. C6): pp. 25. doi:10.1029/2009JC005855.

Trishchenko, A.P. 2019. "Clear-sky composites over Canada from visible infrared imaging radiometer suite to continue MODIS time series." *Canadian Journal of Remote Sensing*, Vol. 45(No. 3–4): pp. 276–289. doi:10.1080/07038992.2019.1601006.

Trishchenko, A.P. 2020. "Probability of the annual minimum snow and ice (MSI) presence over Canada."

Dataset. Version 4. Available at https://open.canada.ca/data/en/dataset/808b84a1-6356-4103-a8e9-db46d5c20fcf.

Trishchenko, A.P., and Garand, L. 2011. "Spatial and temporal sampling of polar regions from two-satellite system on Molniya orbit." *Journal of Atmospheric and Oceanic Technology*, Vol. 28(No. 8): pp. 977–992. Vodoi:10.1175/JTECH-D-10-05013.1.

Trishchenko, A.P., and Garand, L. 2012. "Observing polar regions from space: Advantages of a satellite system on a highly elliptical orbit versus a constellation of low earth polar orbiters." *Canadian Journal of Remote Sensing*, Vol. 38(No. 1): pp. 12–24. doi:10.5589/m12-009.

Trishchenko, A.P., Garand, L., and Trichtchenko, L.D. 2011. "Three-apogee 16-h highly elliptical orbit as optimal choice for continuous meteorological imaging of polar regions." *Journal of Atmospheric and Oceanic Technology*, Vol. 28(No. 11): pp. 1407–1422. doi:10.1175/JTECH-D-11-00048.1.

Trishchenko, A.P., Luo, Y., and Khlopenkov, K.V. 2006. "A method for downscaling MODIS land channels to 250-m spatial resolution using adaptive regression and normalization." Proceedings of SPIE Int. Soc. Opt. Eng., Vol. 6366, 636607. doi:10.1117/12.689157.

Trishchenko, A.P., Luo, Y., Khlopenkov, K.V., Park, W.M., and Wang, S. 2009. "Arctic circumpolar mosaic at 250-m spatial resolution for IPY by fusion of MODIS/TERRA land bands B1–B7." *International Journal of Remote Sensing*, Vol. 30(No. 6): pp. 1635–1641. doi:10.1080/01431160802348119.

Trishchenko, A.P., and Ungureanu, C. 2021. "Minimum snow/ice extent over northern circumpolar landmass in 2000-2019: How much snow survives the summer melt?" *Bulletin of the American Meteorological Society*, Vol. 102(No. 4): pp. E748–E764. doi:10.1175/BAMS-D-20-0177.1.

Trishchenko, A.P., and Wang, S. 2018. "Variations of climate, surface energy budget and minimum snow/ice extent over Canadian Arctic landmass for 2000-2016." *Journal of Climate*, Vol. 31(No. 3): pp. 1155–1172. doi:10.1175/JCLI-D-17-0198.1.

Trishchenko, A.P., Garand, L., and Trichtchenko, L.D. 2019. "Observing polar regions from space: Comparison between highly elliptical orbit and medium Earth orbit constellations." *Journal of Atmospheric and Oceanic Technology*, Vol. 36(No. 8): pp. 1605–1621. doi:10.1175/JTECH-D-19-0030.1.

Trishchenko, A.P., Garand, L., Trichtchenko, L.D., and Nikitina, L.V. 2016. "Multiple-apogee highly elliptical orbits for continuous meteorological imaging of polar regions." *Bulletin of the American Meteorological Society*, Vol. 97(No. 1): pp. 19–24. doi:10.1175/BAMS-D-14-00251.1.

Trishchenko, A.P., Leblanc, S.G., Wang, S., Li, J., Ungureanu, C., Luo, Y., Khlopenkov, K.V., and Fontana, F. 2016. "Variations of annual minimum snow and ice extent over Canada and neighboring landmass derived from MODIS 250-m imagery for 2000–2014." *Canadian Journal of Remote Sensing*, Vol. 42(No. 3): pp. 214–242. doi:10.1080/07038992.2016.1166043.

Trishchenko, A.P., Trichtchenko, L.D., and Garand, L. 2019. "Highly elliptical orbits for polar regions with reduced total ionizing dose." *Advances in Space Research*, Vol. 63(No. 12): pp. 3761–3767. doi:10.1016/j.asr.2019.04.005.

Way, R.G., and Lewkowicz, A.G. 2016. "Modelling the spatial distribution of permafrost in Labrador–Ungava using the temperature at the top of permafrost." *Canadian Journal of Earth Sciences*, Vol. 53(No. 10): pp. 1010–1028. doi:10.1139/cjes-2016-0034.

Wilson, M.J., and Oreopoulos, L. 2013. "Enhancing a simple MODIS cloud mask algorithm for the Landsat data continuity mission." *IEEE Transactions on Geoscience and Remote Sensing*, Vol. 51(No. 2): pp. 723–731. doi:10.1109/TGRS.2012.2203823.

Wolfe, R.E., Lin, G., Nishihama, M., Tewari, K.P., Tilton, J.C., and Isaacman, A.R. 2013. "Suomi NPP VIIRS prelaunch and on-orbit geometric calibration and characterization." *Journal of Geophysical Research (Atmospheres)*, Vol. 118: pp. 11508–11521.

Xiong, X., Che, N., and Barnes, W. 2005. "Terra MODIS on-orbit spatial characterization and performance." *IEEE Transactions on Geoscience and Remote Sensing*, Vol. 43(No. 2): pp. 355–365.

Xiong, X., Che, N., Barnes, W., Xie, Y., Wang, L., and Qu, J. 2006. "Status of Aqua MODIS spatial characterization and performance." Proceedings of SPIE International Society for Optical Engineering, Vol. 6361, 63610T. 9 pp. doi:10.1117/12.687162.

Yu, Y., Stern, H., Fowler, C., Fetterer, F., and Maslanik, J. 2014. "Interannual variability of Arctic landfast ice between 1976 and 2007." *Journal of Climate*, Vol. 27(No. 1): pp. 227–243. doi:10.1175/JCLI-D-13-00178.1.